TCf Manipulation in AlScN Nanomechanical Resonators Using Dual-Mode Parametric Excitation

Yue Zheng, *Graduate Student Member, IEEE*,
Seyyed Mojtaba Hassani Gangaraj, *Graduate Student Member, IEEE*,
Jialin Wang, *Graduate Student Member, IEEE*, Mingyo Park, *Member, IEEE*,
Yifan Fang, *Graduate Student Member, IEEE*, and Azadeh Ansari, *Member, IEEE*

***Abstract*— In this work, we present resonator temperature coefficient of frequency (TCf) manipulation method by using the Duffing nonlinearities and non-dispersive coupling in two resonance modes within the same acoustic cavity. This temperature sensing technique leverages parametric pumping with a lock-in frequency, concurrently inducing signal and idler tones with opposite TCf signs. To demonstrate temperature sensing, aluminum scandium nitride ($Al_{1-x}Sc_xN$) (x = 0.2) drumhead nanomechanical resonators with two resonance modes of vibration (0,1) and (1,1) are fabricated, and the TCf trends of the driven resonance modes and parametrically induced modes are carefully studied. A signal TCf_1 of −178 ppm/K and an idler TCf_2 of +88 ppm/K with a linear trend is experimentally measured, marking the first positive TCf measured on resonators with a negative driven-mode TCf. A one-dimensional lumped parameter model is presented to elucidate the underlying mechanisms of generating opposite TCf signs, showing an excellent match with the measured data. Furthermore, we demonstrate direct TCf manipulations through beat frequency (f_b) modulation, using internal mixing of the induced signals and their harmonics, which can improve the temperature tunability of the resonant system. The presented work drastically simplifies the system-level integration of the resonant sensing systems by eliminating the need for interface electronics and dual feedback loops. [2024-0080]**

***Index Terms*— Temperature sensing, parametric oscillator, aluminum scandium nitride, temperature coefficient of frequency (TCf), cryogenic temperature, dual-mode (DM) modulation, nanoelectromechanical systems (NEMS), piezoelectric thin-film, flexural mode, drumhead resonator.**

I. INTRODUCTION

PARAMETRIC oscillators can be utilized in a wide range of applications in fields such as microwave devices [1], nonlinear optics [2], quantum mechanics [3], [4] and mechanical systems [5], [6]. When a nonlinear material is subjected to intense optical or acoustic wave at the pump frequency (f_{pump}), two in-phase modes can be generated at lower frequencies, referred as signal (f_1) and idler (f_2) which are governed by the law of wave momentum conservation ($f_{pump} = f_1 + f_2$). Simultaneous resonances of both signal and idler frequencies lower the threshold for parametric oscillation and extend the range of frequency tunability when compared to single-resonance based oscillators [7]. Traditional parametric oscillators rely on standalone nonlinear crystals, Dichroic mirrors and solid-state lasers with stringent frequencies and phase-matching conditions under precise temperature control [8]. Recent advancements in nanomechanical systems (NEMS) fabrication of high quality factor (Q) resonators have led to the demonstration of fully integrated cavity- and internal reflection based photonic [2], [9], [10], [11], [12] and phononic [13], [14], [15], [16], [17] parametric oscillators. Most notably, such oscillators take advantage of phenomena such as Kerr and Duffing nonlinearities, four-wave mixing, *etc*.

Recently, there has been a growing interest in using NEMS phononic parametric devices that leverage Duffing nonlinearity for temperature (T) sensing applications. It has been proposed that introducing a parametric pump signal, with a pump frequency as a difference between two fundamental modes ($f_{pump} = f_2 - f_1$), to an electrostatically actuated silicon beam resonator can enhance the temperature sensitivity through the inter-modal coupling [18]. Generating phononic frequency comb, a distinctive state presented in a parametrically amplified system, and tracking the T-dependent spectral line spacing of the resonant sensor can yield remarkable temperature sensitivity [19]. However, in the absence of stabilization technique, frequency combs are also known to be drifting due to environmental perturbations such as ambient pressure and humidity, resulting in phase noise [20], [21]. On the other hand, with different sensitivities of f_1 and f_2 with respect to different physical quantities, a single parametric system can extricate the measurand from environmental perturbation [22]. Despite the advantages of parametric pumping, manipulations of sensitivities in a parametric device without external circuitry is relatively unexplored and it is necessary to understand the underlying sensing mechanisms to advance the resonant phononic parametric temperature sensing technology.

Manuscript received 24 April 2024; revised 10 June 2024; accepted 17 June 2024. Date of publication 25 July 2024; date of current version 3 October 2024. This work was supported in part by the National Science Foundation under Grant ECCS-1542174 and Award CAREER 1944304, and in part by NASA APRA. Subject Editor H. Chang. *(Corresponding author: Yue Zheng.)*

The authors are with the School of Electrical and Computer Engineering, Georgia Institute of Technology, Atlanta, GA 30332 USA (e-mail: yzheng331@gatech.edu).

Color versions of one or more figures in this article are available at https://doi.org/10.1109/JMEMS.2024.3425798.

Digital Object Identifier 10.1109/JMEMS.2024.3425798

1057-7157 © 2024 IEEE. Personal use is permitted, but republication/redistribution requires IEEE permission.
See https://www.ieee.org/publications/rights/index.html for more information.

Authorized licensed use limited to: Georgia Institute of Technology. Downloaded on April 29,2025 at 05:13:13 UTC from IEEE Xplore. Restrictions apply.

In this paper, we present using a single pump frequency to simultaneously induce two modes (0,1) and (1,1) as signal and idler tones on a flexural drumhead resonator made of aluminum scandium nitride ($Al_{1-x}Sc_xN$) as shown in Fig. 1. Using this method, we investigate the T-dependent frequency variation for temperature sensing applications. Firstly, to enhance the sensitivity of temperature sensor, it is important to engineer resonators with high temperature coefficient of frequency (TCf). Typical TCf values of bulk-mode $Al_{1-x}Sc_xN$ resonators previously reported by our group and others range from −25 ppm/K to −60 ppm/K [23], [24], [25], [26], [27], which is inherently limited by the temperature coefficient of elasticity (TCE) of $Al_{1-x}Sc_xN$. It has been shown that device- and circuit-level engineering can be implemented to enhance TCf values [28], [29], [30], [31], [32]. Resonators can be constructed of layers of materials with mismatching thermal expansion coefficients such that additional residual stress can be introduced into the resonators, causing a larger T-dependent resonance frequency shift [28]. Resonance modes, such as flexural mode with fixed boundary conditions, whose resonance frequency possesses a stress-dependent term, can produce a more pronounced frequency shift [29], [33]. Therefore, flexural-mode resonators are a popular choice for stress-enhanced temperature sensing. Alternatively, circuit-level tuning can also enhance temperature sensitivity: a beat frequency (f_b) can be defined as a linear combination of f_1 and f_2 whose scalars can be manipulated to yield high TCf. [30], [31], [32]. The read-out can be achieved by interfacing a dual-mode (DM) oscillator with transimpedance amplifiers (TIAs), multipliers and mixers to form feedback loops which satisfy the Barkhausen stability criterion [32]. However, external CMOS circuitries under industrial temperature standards (−40°C – 85°C) can increase the overall impedance of the system which can introduce thermal noise and delay the read-out [34]. Another challenge arises when f_1 and f_2 have similar TCf values. In this case, defining f_b will provide little impact on improving the overall temperature sensitivity.

In this work, we examine the T-dependent frequency variations of the two parametrically induced signal and idler tones under a locked pump frequency and observe trackable nonlinear mixing tones suitable for direct TCf manipulations. Our group has previously presented the tuning mechanisms of tones and combs formation with non-degenerate pumping on an analogous platform [16] but has not studied the thermal characteristics of the signal/idler tones under parametric excitation. Here, we first show the TCf values of two fundamental modes from 6K to room temperature (300 K) using driven resonance modes. Next, we delineate temperature sensing scheme with parametric pumping and follow up with a physical model capturing the quadratic and cubic nonlinearity required for tone generation. Our solution guarantees two TCf values with opposite signs, whose mixing frequencies allows engineering various TCf values suitable for both sensing and timing/frequency reference applications, without introducing external interface electronics and dual feedback loops required to sustain oscillations of two modes, and thus substantially simplifying the overall circuitry.

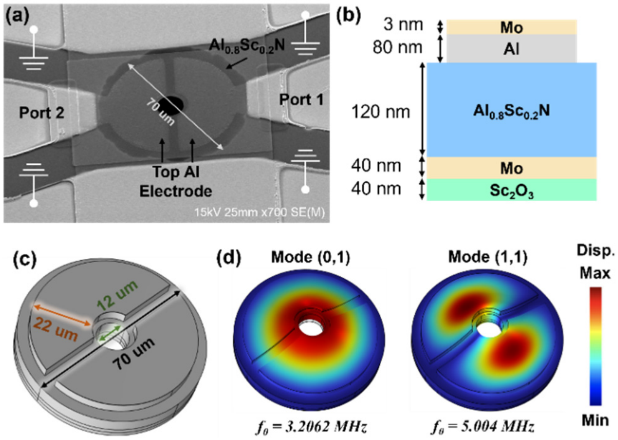

Fig. 1. (a) SEM image of the fabricated flexural-mode drumhead resonator. (b) Cross-sectional schematic of the resonator, showing the material stack compositions and the thicknesses. (c) Geometry for the COMSOL eigenfrequency simulations and (d) simulated flexural mode shapes of mode (0,1) and mode (1,1) which are used for dual-mode parametric excitation. The simulated eigenfrequencies are matched with measurement results with less than 5% of error.

II. PRINCIPLES TEMPERATURE SENSING WITH DUAL-MODE PARAMETRIC EXCITATION

The parametric wave degeneration phenomenon allows simultaneous generation of two modes with one frequency input using a traditional pump-probe approach. Dual-harmonic generation through nonlinear wave interaction has already been demonstrated in optical [35] and acoustic [16] domains. Here, we use the pump-probe approach and blue sideband excitation to create a sensing scheme where f_1 and f_2 oppositely vary with temperature, ensuring both modes provide TCfs with opposite signs. The opposite frequency shifts can be achieved by fixing the pump frequency f_{pump} (angular frequency ω_p) and monitoring the change of f_1 and f_2 with temperature. Fig. 2(a) illustrates the parametric temperature sensing scheme using blue sideband excitation under a lock-in $f_{pump} = f_1 + f_2$: when the ambient temperature changes from the reference level T_0 by the amount of ΔT, an intermodal wave momentum ($\Delta\omega(T)$) is transferred from the more energetic mode to the other [18], yielding two tones with angular frequencies of $\omega_1(T_0) - \Delta\omega(T)$ with a negative rate of change and $\omega_2(T_0) + \Delta\omega(T)$ with a positive rate of change. The conservation can be described with the following equation:

$$\begin{aligned}\omega_1(T_0)+\omega_2(T_0) &= (\omega_1(T_0)-\Delta\omega(T))+(\omega_2(T_0)+\Delta\omega(T)\\ &= \omega_1(T)+\omega_2(T)=\omega_p. \qquad (1)\end{aligned}$$

The temperature will perturb the amount of $\Delta\omega(T)$ through resonant induced friction between the two modes and stiffness coupling, which will be elaborated in the model in Section V.

To execute our proposed sensing scheme, we inject a single frequency tone with frequency f_{pump} to the resonator at the input port and use a spectrum analyzer to monitor the signal amplitude of the entire frequency spectrum (Fig. 2(b)). Although constructing a phased-locked loop using lock-in amplifier, local oscillator and phase comparator can be deployed for practical read-out of a sensor [22], a benchtop spectrum analyzer is a robust option to stabilize and read-out

Authorized licensed use limited to: Georgia Institute of Technology. Downloaded on April 29,2025 at 05:13:13 UTC from IEEE Xplore. Restrictions apply.

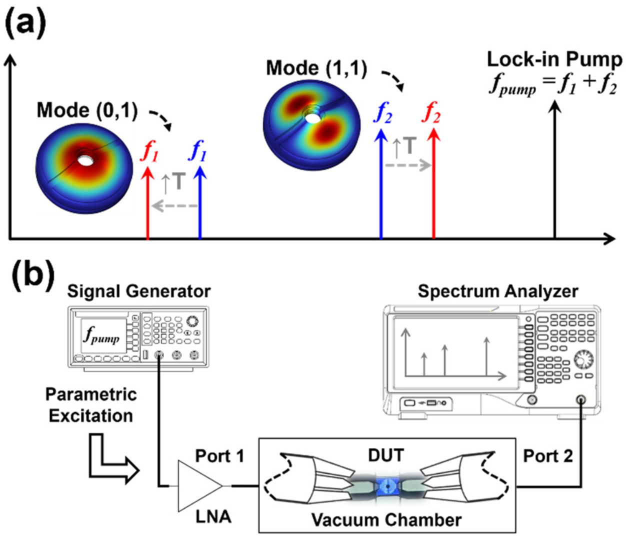

Fig. 2. (a) Working principle of the parametric temperature sensing: two parametric tones f_1 and f_2 are generated when the parametric pump frequency is at the sum of the resonance frequency of the two flexural mechanical modes. While the value of pump frequency f_{pump} is set fixed, f_1 and f_2 shift up and down as the ambient temperature increases. (b) Measurement setup for the parametric tones generation.

multiple frequencies at a wide range of spectrum for in-house characterization. With the internal mixer, embedded voltage-controlled oscillator (VCO) and external frequency reference, the N9030B spectrum analyzer used in our experiments can provide a counter resolution up to 0.001 Hz [36].

III. ALUMINUM SCANDIUM NITRIDE DRUMHEAD RESONATOR CHARACTERIZATION

To demonstrate temperature sensing with DM parametric excitation technique, we design and fabricate flexural-mode circular drumhead resonators with $Al_{0.8}Sc_{0.2}N$ piezoelectric thin film. COMSOL finite element analysis (FEA) is performed to identify the mode shapes of the two resonance modes. In the next section, we characterize the driven resonance modes of the fabricated $Al_{0.8}Sc_{0.2}N$ flexural-mode resonator. A very large TCf value (up to -1022 ppm/K at 300 K) is observed as a result of thermally induced residual stress. We further present dual-tone excitation and study the frequency signatures in the temperature range of 260 K $\sim$ 300 K and demonstrate TCf manipulation using the parametric approach with nonlinear-mode mixing.

A. $Al_{0.8}Sc_{0.2}N$ Thin-Film Growth

A 120 nm-thick $Al_{0.8}Sc_{0.2}N$ piezoelectric thin-film layer is grown on a 40nm/40nm molybdenum (Mo)/scandium oxide (Sc_2O_3) on silicon (Si) using a Veeco GENxplor molecular beam epitaxy (MBE) system at the University of Michigan. The piezoelectric layer is epitaxially terminated with an 80 nm-thick Al layer. To minimize the oxidation of Al, a thin layer (3 nm) of Mo is deposited to passivate the top Al. Fig. 1(b) illustrates the cross-sectional material stacks prepared for the flexural-mode resonators fabrication.

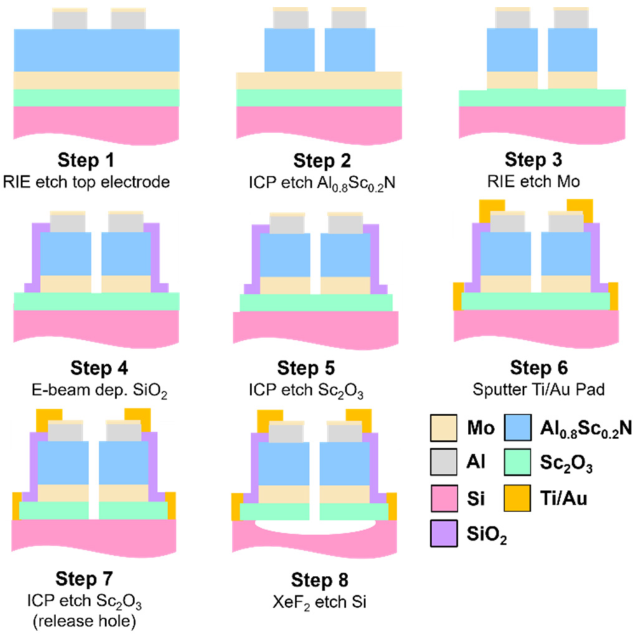

Fig. 3. $Al_{0.8}Sc_{0.2}N$ flexural-mode circular drumhead resonator fabrication flow.

B. Fabrication Process of Flexural-Mode Resonators

The fabrication process flow is outlined in Fig. 3. To define the top electrodes, the top Mo/Al layer is patterned and etched using reactive ion etching (RIE) with CF_4-based plasma (step 1). The $Al_{0.8}Sc_{0.2}N$ film is etched using inductively coupled (ICP) etching with a $BCl_3/Cl_2/Ar$ plasma (step 2). The bottom Mo layer is then etched using RIE to define the bottom electrodes (step 3). Next, the $Al_{0.8}Sc_{0.2}N$ body and bottom electrodes are passivated with silicon dioxide (SiO_2) deposited using electron beam evaporator (step 4). The Sc_2O_3 layer is etched using ICP to expose the Si device layer (step 5). Subsequently, the Ti/Au metal contact pads are sputter deposited (step 6). The Sc_2O_3 layer is ICP etched again to expose the Si layer for device release (step 7). In step 2, 3 and 7, a small circular release hole with a diameter of 12 um is opened at the center of the resonator for a more controlled circular cavity definition during the subsequent isotropic Si device layer release using Xactix xenon difluoride (XeF_2) etcher (step 8). The resulting cavity size has a diameter of 70 um, as shown in the SEM image of the fabricated resonator (Fig. 1(a)).

C. Design Verification With Finite Element Analysis (FEA)

COMSOL Multiphysics is used to simulate the two flexural mode shapes in order to match the resonance frequencies observed from the driven-mode characterization. Fig. 1(c) shows the COMSOL geometry annotated with the dimension of the device, which are confirmed from the SEM image. An inherent tensile in-plane stress of $\sim$550 MPa, which is induced due to the high-temperature nature of the MBE film growth, is considered in the model. The stress value is comparable to the value reported in [37] and [38]. The first two simulated mechanical resonance modes are mode (0,1) and mode (1,1), whose simulated resonance frequencies

Authorized licensed use limited to: Georgia Institute of Technology. Downloaded on April 29,2025 at 05:13:13 UTC from IEEE Xplore. Restrictions apply.

are 3.2062 MHz and 5.004 MHz (Fig. 1(d)), matching our measured response.

IV. TEMPERATURE MEASUREMENTS OF THE RESONATORS

A. Measurement Setup

The fabricated flexural resonators are tested with ground-signal-ground (GSG) probes in an Advanced Research System PS-L Flow Cryostat probe station under vacuum condition. The temperature of the cryostat is cooled down to 6K with a Sumitomo F-70 water-cooled helium compressor.

For the driven-mode characterization, the transmission coefficient S_{21} is recorded by a Keysight E5071C vector network analyzer (VNA). To enhance the signal to noise ratio and to amplify the RF power input of the resonator as necessary for the minimum excitation threshold of the parametric pumping, a Mini-Circuits ZFL-1000LN+ low-noise amplifier (LNA) operated at 15V of DC voltage is connected between port 1 and VNA, providing approximately 23 dB of amplification.

For the two-tone parametric excitation, pump-probe approach is applied to monitor the pump signal at f_{pump} and the two induced parametric tones at f_1 and f_2: port 1 of the resonator is connected to a Keysight 5173B EXG signal generator, which functions as a single-tone electric pump, while port 2 is coupled to a Keysight N9030B PXA spectrum analyzer (Fig. 2(b)).

B. Characterization of Temperature-Dependent Driven Resonance Modes

The linear frequency responses of the two driven mechanical resonance modes are measured at room temperature (300 K) (Fig. 4(a) and (b)). Resonance frequencies (f_m) and $Q_{-3\text{dB}}$ are extracted from the linear responses of each mode. The Lorentz fitting of the driven frequency response reveals that linear resonance frequency for mode (0,1) (f_{m1}) and for mode (1,1) (f_{m2}) are 3.202 MHz with a $Q_{-3\text{dB}}$ of 753 and 4.918 MHz with a $Q_{-3\text{dB}}$ of 1438 respectively.

Next, we investigate the amplitude-frequency (A-f) characteristics to analyze the sources of nonlinearities present in the resonators. The S_{21} frequency response curves of mode (1,1) under various input RF power are obtained by performing a forward frequency sweep at room temperature (Fig. 4(c)). In our study, RF power (P_{in})-induced Duffing nonlinearities that contribute to the skewness of the S_{21} frequency curve are observed. They can be sourced to the geometric structure (*e.g.* clamping and ultra-thin film) that caused large deformation (geometric), nonlinear dependence of elastic constants on stress-strain relationship (material), and self-heating (thermal) [39]. At low P_{in} (−49 dBm to −47 dBm), the spring softening effect occurs and the resonance frequency decreases, which is caused by the self-heating effect. As the power increases further, nonlinear mechanical hardening dominates due to the geometric nonlinearity. The power threshold of bifurcation starts above −39 dBm of P_{in} for mode (1,1).

To quantify the contribution of resonance frequency changes due to self-heating and to validate that geometric nonlinearity dominates at the RF power range of interest, we construct a heat-transfer model of the resonator in COMSOL using the method presented in [40] and [41] to evaluate the power-dependent maximum self-heating temperature rise (ΔT_{self}) by applying a boundary heat source to one of the top electrodes of the resonator for RF power input and a referenced-temperature (293.15 K) boundary condition at the periphery of the resonator (Fig. 4(d)). The input values of the boundary heat source are determined by the dissipative heat power (P_{diss}) calculated by using S-parameters from measurements with consideration of LNA gain (G_{LNA}): $P_{\text{diss}} = (P_{\text{in}} \cdot G_{\text{LNA}})(1\text{-}|S_{21}|^2\text{-}|S_{11}|^2)$ [42]. The modeled ΔT_{self} using FEA can be then described by: $\Delta T_{\text{self}} = P_{\text{diss}} \cdot R_{\text{th}}$, where R_{th} is the thermal resistance of the structure [43]. The extracted R_{th} of the resonator is around 9.22×10^3 K/W. Thus, the temperature rise on our resonator platform due to self-heating effect is minimal, as ΔT_{self} does not rise beyond 2 K while operating at the RF power of interest. This is due to the resonator being anchored all around which creates a broad heat dissipation path that gives rise to a smaller R_{th} compared to resonators with suspended anchors ($\sim 10^4$K/W) [40] in which the self-heating can predominantly induce nonlinearities.

To show the temperature sensitivity of the resonator under uncoupled state, the standalone linear-mode temperature sensitivities of mode (0,1) and mode (1,1) are characterized when the ambient temperature changes from 6K to 300 K. The extracted normalized frequency change ($\mathrm{d}f/f$) under this temperature range for mode (0,1) and mode (1,1), which are shown in Fig. 4(e) and (f). TCf is evaluated using: $\text{TC}f = (1/f)(\mathrm{d}f/\mathrm{d}T)$. the TC$f$ for mode (0,1) ($\text{TC}f_{(0,1)}$) and for mode (1,1) ($\text{TC}f_{(1,1)}$) are −898 ppm/K and −1022 ppm/K at 300K. For comparison, the TCf of an $\text{Al}_{0.7}\text{Sc}_{0.3}\text{N}$ film bulk acoustic resonator (FBAR) has been reported to be −30.1 ppm/K [25]. Similar values have been reported for $\text{Al}_{1-x}\text{Sc}_x\text{N}$-based surface acoustic wave (SAW) resonators and contour-mode resonators (CMRs) [27], [44]. In comparison, a few works reported the TCf values of stress-enhanced AlN flexural-mode resonators to be −391 ppm/K [45], −512 ppm/K [46] and −710 ppm/K [47]. The TCf of flexural-mode resonators can transcend the material limit because (1) the resonance frequency of flexural mode has a stress dependency that further softens the elasticity with increasing temperature [48] and (2) the thermally induced compressive stress is accumulated in the active device area since the entire frame of the membrane is anchored with the rest of the substrate.

To verify that thermal stress is the main contributor to the large driven-mode TCf of the flexural-mode resonator, we follow the approach in [49] and [50], and develop a model in COMSOL to predict the TCf behavior, considering the TCE, coefficient of thermal expansion (α) and compressive stress (σ). A fixed boundary condition is applied at the far end of each resonator which occupies an area of approximately 150×150 um^2. Using our simulation model, we compute the resonance frequency at different temperatures due to thermal residual stress by enabling the thermal expansion feature in the Solid Mechanics interface. In the model, the strain induced by thermal expansion (ϵ_{th}) is calculated by $\epsilon_{\text{th}} = \alpha(T) \cdot (T\text{-}T_{\text{ref}})$,

Authorized licensed use limited to: Georgia Institute of Technology. Downloaded on April 29,2025 at 05:13:13 UTC from IEEE Xplore. Restrictions apply.

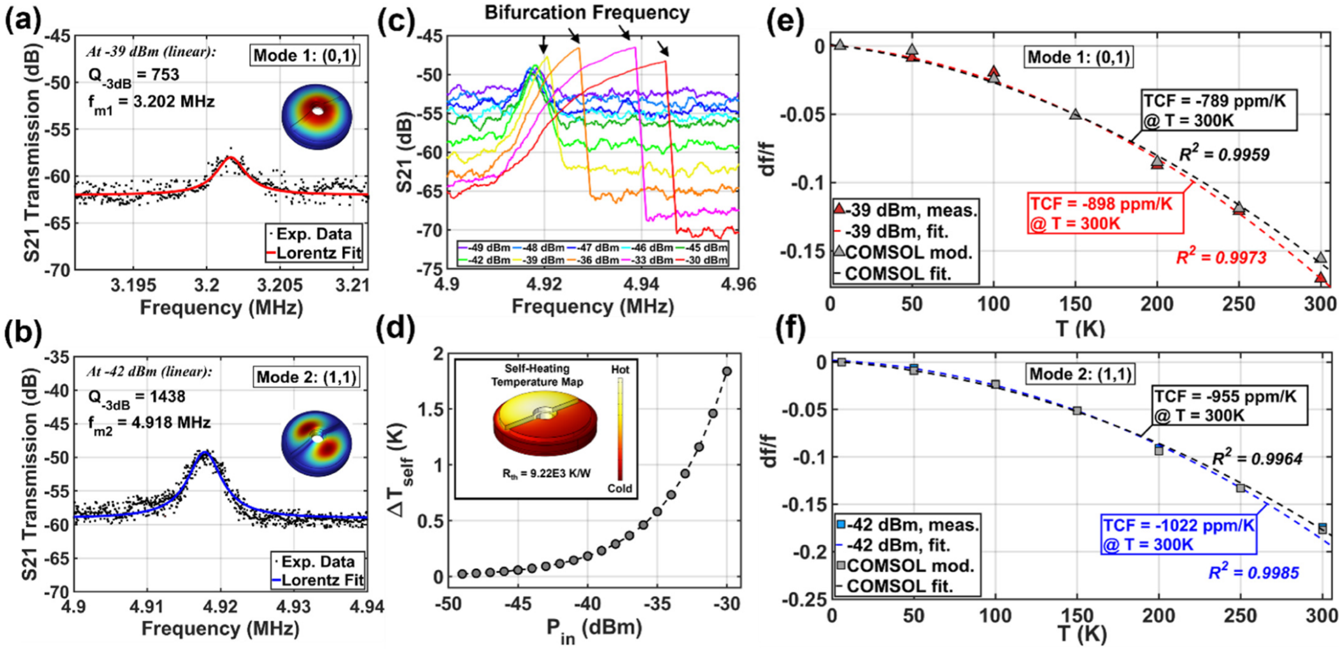

Fig. 4. Linear responses of (a) mode (0,1) and (b) mode (1,1) at room temperature (300 K). (c) Driven-mode characterization of mode (1,1) at various input RF power level at room temperature. (d) FEA simulated maximum temperature rise (ΔT_{self}) with respect to input RF power (P_{in}). The inset shows the temperature distribution of the flexural-mode drumhead resonator, with an extracted thermal resistance of 9.22E3 K/W. Extracted df/f for (e) mode (0,1) and (f) mode (1,1) from the temperature measurements, compared with the results obtained from COMSOL pre-stressed eigenfrequency simulation. At room temperature (300 K), the linear-mode $TCf_{(0,1)}$ and $TCf_{(1,1)}$ are -898 ppm/K and -1022 ppm/K.

where T_{ref} is the film deposition temperature. With the thermal stress resolved, the shift in resonance frequency due to thermal-softening effect can be computed by using the pre-stressed eigenfrequency study. Fig. 4(e) and (f) also present the normalized frequency change df/f with respect to temperature for mode (1,1) predicted using the COMSOL model compared with the experiment results. The model assumes a deposition temperature T_{ref} of 1100 °C, an inherent tensile in-plane stress of ∼550 MPa and T-dependent α values obtained from of the AlScN film [51]. The modeled trend shows reasonable agreement with the experiment results.

C. Temperature Sensing Using Dual-Mode Parametric Tone Excitation

In this section, we demonstrate the temperature sensitivity of the two fundamental tones from the dual-mode parametric excitation experiment. Fig. 5(a) shows an example of the power spectrum from 1MHz to 10 MHz at a temperature of 260 K when the pump frequency is locked at 8.8 MHz and the pump power is +5 dBm. The observable peaks can be generally classified into four categories: (1) fundamental pump tone at f_p and its harmonics at multiples or half of f_p, (2) fundamental idler tone at f_1 and its harmonics at multiples of f_1, (3) fundamental signal tone at f_2 and its harmonics at multiples of f_2 and (4) mixing tones of f_1 and f_2. As a minimum power threshold for the parametric excitation, a pump power (P_{pump}) of -3 dBm, or equivalently 20 dBm of incident power (P_{pump}^{inc}), is required to parametrically induce the signal and idler tones. Fig. 5(b) shows the measured Arnold's tongue, mapping four observed parametric states, which were reported in our previous work [16], as a combination of input pump power and detuning pump frequency at 300 K. The pump frequency of the parametric temperature sensor is chosen to be the region where neither combs nor chaos is forming. It can be observed that the widest frequency dynamic range (8.64 MHz to 8.8 MHz) occurs at a P_{pump} of +5 dBm. We further repeat the process by decreasing the ambient temperature with a temperature step of 10 K. Considering the driven mode characterization results, f_{m1} and f_{m2} both increase as the ambient temperature decreases. Since f_{pump} is near $f_{m1} + f_{m2}$, the detuning range also moves down as the ambient temperature cools down. To maximize the temperature detection range of the resonator, f_{pump} is fixed to 8.8 MHz in the following study of the temperature sensitivities of signal and idler tones. Fig. 5(c) and (d) present the shifting of the resonance frequency of signal f_1 and idler f_2 when temperature decreases from 300 K to 260 K, showing that f_1 monotonically decreases with temperature while f_2 behaves the opposite way. It can be noticed that a discrete jump of the frequency occurs at T = 270 K. Such observation was also reported in other pump-probe systems [52], [53], and is a characteristic when the device oscillation is near a static bifurcation point [52]. The extracted TCfs of f_1 and f_2 are -178 ppm/K and $+88.4$ ppm/K at 300 K. To understand the amount of frequency perturbation on the two tones due to varying RF pump power, we repeated the measurement with an input RF power ranging from -3 dBm to +7dBm, with less than 6% of change of the TCf observed for each tone. The small variations are likely due to the self-heating effect. To understand the temperature trend of the frequency shift of each mode, we will present a physical and analytical model to corroborate our findings in the next section.

Authorized licensed use limited to: Georgia Institute of Technology. Downloaded on April 29,2025 at 05:13:13 UTC from IEEE Xplore. Restrictions apply.

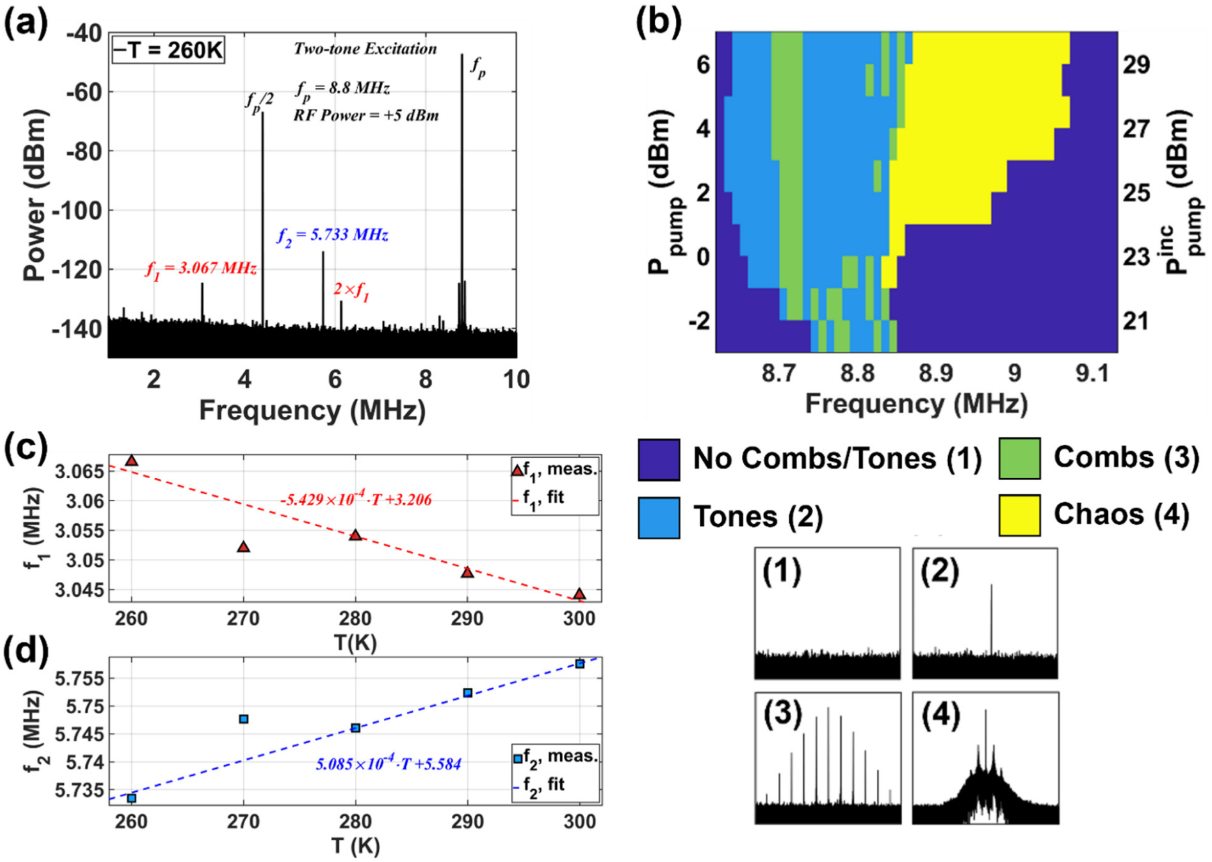

Fig. 5. (a) Measured power spectrum from 1 MHz to 10 MHz of the parametric excitation at a fixed pump frequency f_{pump} of 8.8 MHz at 260K with a pump power of +5 dBm. (b) Measured Arnold's tongue, mapping different dynamic states of detuning pump frequency and drive power at room temperature. Frequency shifts of two parametric tones with varying temperature: extracted TCf of (c) tone f_1 with TC$f_1 = -178$ ppm/K, and (d) tone f_2 with TC$f_2 = +88.4$ ppm/K.

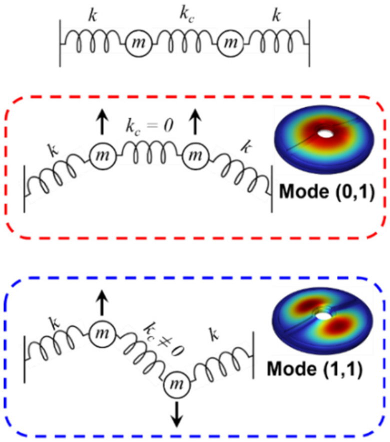

Fig. 6. 1D 2DoF mass-spring model of the flexural-mode resonator. Motions of mode (0,1) and mode (1,1) can be approximated as two equivalent masses moving unidirectionally and antithetically.

V. Comprehensive Study of Dual-Mode Parametric Excitation

A. Physical Modeling

Parametric excitation of two tones has been modeled in various mechanical systems in the past [54], [55], [56]. Among these studies, the presence of nonlinear terms and mode coupling in the equations of motion is essential for generating signal and idler modes under parametric pumping. Notably, prior research has employed the Fermi-Pasta-Ulam (FPU) model to solve the mode equations. In the most general scenario, equations of motion for N-coupled modes can be solved using the Poincaré-Lindstedt (PL) perturbation method, as demonstrated by [57].

For instance, to model parametric excitation in resonant mechanical systems, Ganesan and Seshia [58] discuss a generalized FPU mode equation. This FPU model is a high-level mathematical formulation encompassing all possible coupling terms. To simplify this and tailor it to our two-coupled mode resonant system, we introduce a simplified two-degree-of-freedom model, with two masses and three nonlinear springs as detailed below. We show that our model well matches the measured results.

Fig 6. shows our one dimensional two degrees of freedom (DoF) physical model, in which each mass represents one half of the circular resonator, moving unidirectionally/antithetically in the two resonance modes (0,1)/(1,1). These two resonators are connected symmetrically through the central section of the drumhead. The model consists of two identical masses m, each representing one half of the resonator, and three springs. The springs on the left and right sides are identical with stiffness of k and damping of c, and the middle spring has a stiffness of k_c and damping of c_c. The mass of the resonator is equal to $2m$ and the numerical value of m is shown in table I. The

Authorized licensed use limited to: Georgia Institute of Technology. Downloaded on April 29,2025 at 05:13:13 UTC from IEEE Xplore. Restrictions apply.

mass is calculated based on the structural design and material properties of the resonator. Mathematical model for coupled resonator has been developed by Li et. al. [18], but the key difference between the mentioned study and the presented model in this paper is the inclusion of nonlinearities in the equations of motion (EoM). Our approach has been previously employed in the analysis of coupled resonators [59], [60], [61]. In our model, the springs are assumed to be nonlinear, leading to the emergence of the coupling terms presented in (5) and (6), which are necessary to describe the behavior of the signal/idler modes.

The nonlinear terms in the springs have the form of quadratic and cubic nonlinearity [62], originating from the material and structural nonlinearities [62], incorporated in the stiffness of the structure [63]. This nonlinear form yields to a nonlinear spring constant as shown in (1). In the equation of motion, αk is referred to as k_2 and βk is referred to as k_3.

$$k_{(x)} = k(1 + \alpha x + \beta x^2) \tag{2}$$

The EoMs used to describe the behavior of the resonator are shown in (3), where $x_{1,2}$ are the displacements of each mass.

$$\begin{aligned} &m\ddot{x}_1 + k_{(T)}x_1 - f_{T1}(t) + k_{2_{(T)}}x_1^2 + k_{3_{(T)}}x_1^3 + c\dot{x}_1 + k_{c_{(T)}} \\ &\quad \times (x_1 - x_2) + k_{c2}(x_1 - x_2)^2 + k_{c3}(x_1 - x_2)^3 + c_c(\dot{x}_2 - \dot{x}_1) \\ &= F_1 cos\left(\omega_p t\right), \end{aligned} \tag{3.1}$$

$$\begin{aligned} &m\ddot{x}_2 + k_{(T)}x_2 - f_{T2}(t) + k_{2_{(T)}}x_2^2 + k_3 x_2^3 + c\dot{x}_2 + k_{c_{(T)}(x_2 - x_1)} \\ &\quad + k_{c2}(x_2 - x_1)^2 + k_{c3}(x_2 - x_1)^3 + c_c(\dot{x}_2 - \dot{x}_1) \\ &= F_2 cos\left(\omega_p t\right), \end{aligned} \tag{3.2}$$

where k_2 and k_3 are the first and the second order corrections for two springs at each end, k_{c2} and k_{c3} are the first- and the second-order corrections for the coupling spring, F_1 and F_2 are the forces applied to the first mass and the second mass respectively, and ω_p is the pump angular frequency. The effect of temperature is incorporated through k and k_c. The EoMs can model two natural modes of the system, which are shown in Fig. 6. Resonant induced friction force (RIFF) is added to the equations of motion to compensate for the absorbed power which leads to a temperature change due to local heating [33], [64]. The frequencies of these modes and the RIFF are described below:

$$\omega_1 = \sqrt{k/m}, \tag{4.1}$$

$$\omega_2 = \sqrt{(k + 2k_c)/m}, \tag{4.2}$$

$$f_{T_{1,2}}(t) = 2m\omega_{1,2}\lambda_\omega\lambda_T[F(t)\dot{x}_{1,2}]_{avg}x_{1,2}, \tag{4.3}$$

$f_{T1,2}(t)$ is a form of RIFF which is due to the internal friction of the solids. λ_ω, and λ_T are characteristic constants. λ_ω depends on the material and spatial structure of vibration modes and it relates temperature change. λ_T relates the input power to temperature change of the resonator [64]. The damping coefficients c and c_c are related to the quality factor of mode (0,1) and mode (1,1), Q_1 and Q_2, by

$$c/m = \omega_1/Q_1, \tag{5.1}$$

$$(c + 2c_c)/m = \omega_2/Q_2. \tag{5.2}$$

TABLE I
PARAMETERS USED IN NUMERICAL SIMULATIONS

Symbol	Unit	Value	Symbol	Unit	Value	Symbol	Unit	Value
m	kg	1.5×10^{-12}	k	N/m	varied	k_c	N/m	varied
c	N·m/s	1.3×10^{-8}	k_2/k	-	3×10^5	k_{c2}/k_c	-	0
c_c	N·m/s	9×10^{-10}	k_3/k	-	1×10^5	k_{c3}/k_c	-	0

In equations (4.1) and (4.2), k and k_c are calculated based on measuring ω_1 and ω_2 using driven-mode excitation. The modal equation of motion can be derived using normal coordinates instead of x coordinates. The normal coordinates are defined as $X_1 = x_1 + x_2$ and $X_2 = x_1 - x_2$. $X_{1,2}$ are the displacements of the mode corresponding to mode (0,1) and (1,1). By adding and subtracting the EoMs, we can rewrite the equations with normal mode coordinates shown in (6.1) for mode (0,1) and (6.2) for mode (1,1).

$$\begin{aligned} &\ddot{X}_1 + \omega_{1_{(T)}}^2 X_1 - F^*_{RIFF,X_1} + \frac{\omega_{1(T)}}{Q_1}\dot{X}_1 + \frac{k_{2(T)}}{2m}X_1^2 \\ &\quad + \left(\frac{k_{2(T)}}{2m} + \frac{2k_{c2}}{m}\right)X_2^2 + \frac{k_{3(T)}}{4m}X_1^3 + \frac{3k_{3(T)}}{4m}X_1X_2^2 \\ &= A_1^* cos\left(\omega_p t\right), \end{aligned} \tag{6.1}$$

$$\begin{aligned} &\ddot{X}_2 + \omega_{2_{(T)}}^2 X_2 - F^*_{RIFF,X_2} + \frac{\omega_{2(T)}}{Q_2}\dot{X}_2 + \left(\frac{k_{3(T)}}{4m} + \frac{2k_{c3}}{m}\right) \\ &\quad \times X_2^3 + \frac{k_{2(T)}}{m}X_2X_1 + \frac{3k_{3(T)}}{4m}X_2X_1^2 \\ &= A_2^* cos\left(\omega_p t\right), \end{aligned} \tag{6.2}$$

where $A_1 = F_1 + F_2$, $A_2 = F_1 - F_2$, $A_i^* = A_i/m$, and $F^*_{RIFF,X_i} = \frac{F_{RIFF,X_i}}{m}$, $i = 1, 2$. While second- and third-order corrections of the coupling spring are also temperature dependent, in our presented model they are set to be zero. Since nonlinear behavior of the side springs has been shown to adequately model the measured results, the nonlinearities of the coupling spring are neglected. These parameters are retained in the equations to demonstrate their roles in tuning different terms of the equation. The high-order cubic/quadratic terms describe the nonlinear dynamics and coupling between modes. Both are critical to parametrically couple mode (0,1) and mode (1,1) and generate the signal/idler tone. The cubic and quadratic Duffing nonlinearity α_{cubic} and $\alpha_{quadratic}$ of each mode and the dispersive coupling $\gamma_{12(21)}$ can be expressed as

$$\alpha_{cubic,1} = k_3/4, \tag{7.1}$$

$$\alpha_{cubic,2} = k_3/4 + 2k_{c3}, \tag{7.2}$$

$$\alpha_{quadratic,1} = k_2/2 + 2k_{c2}, \tag{7.3}$$

$$\alpha_{quadratic,2} = 0, \tag{7.4}$$

$$\gamma_{12} = \gamma_{21} = 3k_3/4. \tag{7.5}$$

As shown in equations (7.1) to (7.5), two modes of vibration are mechanically coupled through nonlinearities of the springs.

The frequency response of the system is simulated by numerically solving the coupled equations using MATLAB when the resonator is parametrically excited ($\omega_p = \omega_1 + \omega_2$).

Authorized licensed use limited to: Georgia Institute of Technology. Downloaded on April 29,2025 at 05:13:13 UTC from IEEE Xplore. Restrictions apply.

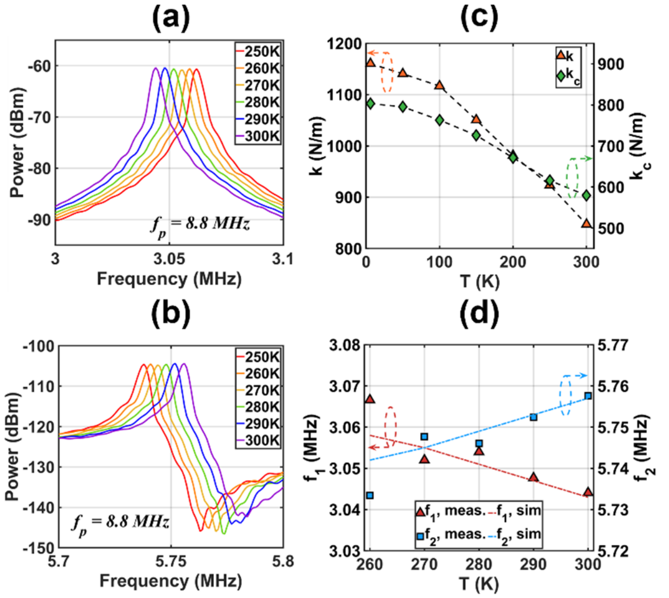

Fig. 7. Numerical simulations of the power spectrum modeling (a) f_1 and (b) f_2 excitation at a fixed pump frequency f_{pump} of 8.8 MHz when temperature varies from 250 K to 300 K. (c) Variations of equivalent values of k and k_c calculated based on driven-mode resonance frequencies f_{m1} and f_{m2} with respect to temperature. (d) Comparison of simulation and measurement trends of f_1 and f_2 vs. temperature.

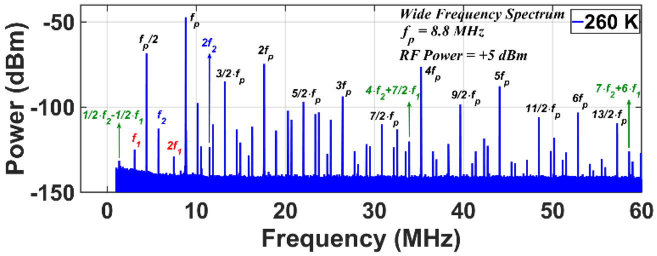

Fig. 8. Measured wideband power spectrum of the parametric excitation at a fixed pump frequency f_{pump} of 8.8 MHz at 260K with a pump power of +5 dBm (green: mixed tones reported in Table II, red/blue: fundamental tones and their harmonics, black: pump frequency and its harmonics).

TABLE II

EXTRACTED BEAT FREQUENCY SENSITIVITY BY MIXING DUAL-MODE TONES FROM MEASUREMENTS ($T = 300$ K)

	a	b	f_b (MHz)	TCf_b calc. (ppm/K)	TCf_b meas. (ppm/K)
Timing	3.5	-4	33.598	3.951	4.982
	6	-7	59.939	0.487	1.173
Sensing	2	1	0.3492	-4555	-
	-1/2	-1/2	1.3469	+389	+448.25

In order to solve the equation, the parameters are calculated based on the driven mode experiments and then used to simulate the behavior of the system in parametric excitation. The quality factors are assumed to remain constant as the temperature changes.

Table I shows the modeled mass, linear and nonlinear spring coefficient, and damping coefficients used in the model. The nonlinear terms affect the frequency response by exchange of energy between oscillation modes via inter-modal coupling [65]. Fig. 7 shows the result for the parametric excitation. It is shown that f_1 decreases as the temperature increases whereas f_2 increases (Fig. 7(a) and (b)). These changes in natural frequencies are such that the summation of two frequencies remains the same as the pump frequency. Fig. 7(c) shows the equivalent k and k_c calculated in the parametric excitation. The equivalent k decreases with increase of the temperature due to softening of the material. Conversely, the equivalent k_c increases due to nonlinear effects of k. k_c can be assumed as a mechanism that couples two modes of vibration. The changes of f_1 and f_2 as a function of temperature is shown in Fig. 7(d), showing an excellent match between the measured and simulated frequencies vs. temperature.

VI. A REFERENCE-FREE RESONANT TEMPERATURE SENSING/FREQUENCY STABILIZATION APPROACH

In this section, we demonstrate the versatility of temperature sensing using DM parametric tones excitation to generate various TCf values suitable for different application requirements. Large TCf is critical to enhance the sensitivity and resolution of temperature sensing applications while a zero TCf is desirable for frequency stabilization. In prior work, TCf manipulation using a DM resonator system is achieved by defining a beat frequency f_b as a linear combination of f_1 and f_2 [30], [32]:

$$f_b = a \cdot f_1 - b \cdot f_2, \tag{8}$$

where a and b are multiplicative constants which are integers or halves. In our solution, a and b correspond to the subharmonics of f_1 and f_2. The mixed harmonics (e.g., $f_2/2 + f_1/2$) observed in measurements are visible from 1.34 MHz up to 59.94 MHz (Fig. 8), thus one can directly mix these harmonics to generate the beat frequency without the requirement of designing an oscillator circuitry or frequency multipliers. The beat frequency sensitivity TCf_b is given by substituting (7) into the of TCf:

$$TCf_b = \frac{1}{f_b}(a \cdot f_1 \cdot TCf_1 - b \cdot f_2 \cdot TCf_2). \tag{9}$$

Using our measured f_1, f_2, TCf_1, TCf_2 presented in Fig. 5 and (9), we enumerate and measure the a few beat frequencies whose sensitivities are suitable for either timing or sensing applications by mixing the first- and second-order harmonics (Table II). It should be noted that these mixing combinations (except for the case that $a = 2$ and $b = 1$) of tones are observed in our measurements. The measured TCf_b values tend to be slightly higher possibly due to the ambient temperature variation from the power setting and electrical noise but overall agree well with the predictions.

Although the presence of f_1 and f_2 relies on nonlinear operation of the resonator, the DM parametric system shows great potential as a temperature-stable reference or a temperature sensor. The highest extracted TCf_b is −4555 ppm/K, which is twice as large as the TCf observed in driven-mode response.

Authorized licensed use limited to: Georgia Institute of Technology. Downloaded on April 29,2025 at 05:13:13 UTC from IEEE Xplore. Restrictions apply.

VII. Conclusion

In this study, we performed thermal characterization of DM $Al_{0.8}Sc_{0.2}N$ flexural-mode drumhead resonator. We determined the temperature coefficient of frequency values using driven-mode approach, showing large TCf values (~ -1000 ppm/K). We developed a novel temperature-sensing technique that utilizes beat frequency modulation to engineer various temperature coefficient of frequency values. This technique introduces signal and idler tones with opposing temperature coefficient of frequencies. We demonstrated parametric excitation in the temperature range of 260 K to 300 K under locked f_p, showing a linear relationship between temperature and the frequencies of the tones. A proposed 1D lumped parameter mass-spring model has helped elucidate the nonlinear dynamics explaining the temperature-dependent frequency drifting of these tones. Through beat frequency modulation, our approach can double the temperature coefficient of frequency but also simplify the electronic circuitry without constructing oscillators. This opens up new opportunities to simplify and enhance the design, production, and application of temperature-sensing devices in future.

Acknowledgment

The authors would like to acknowledge Prof. Z. Mi and members of his research group for performing the $Al_{0.8}Sc_{0.2}N$ MBE growth and IQE plc., for providing the Mo/Sc_2O_3 on Si base template. They want to express their gratitude for the fabrication support from the Institute for Electronics and Nanotechnology (IEN) cleanroom facility at Georgia Institute of Technology, a member of the National Nanotechnology Coordinated Infrastructure (NNCI). They also thank NASA for sponsoring this project.

References

[1] K. Numata, S. Wu, and H. Riris, “Fast-switching methane LiDAR transmitter based on a seeded optical parametric oscillator,” *Appl. Phys. B, Lasers Opt.*, vol. 116, no. 4, pp. 959–966, Sep. 2014.

[2] G. Marty, S. Combrié, F. Raineri, and A. De Rossi, “Photonic crystal optical parametric oscillator,” *Nature Photon.*, vol. 15, no. 1, pp. 53–58, Dec. 2020.

[3] P. Kinsler and P. D. Drummond, “Quantum dynamics of the parametric oscillator,” *Phys. Rev. A, Gen. Phys.*, vol. 43, no. 11, pp. 6194–6208, Jun. 1991.

[4] O. Morin, V. D’Auria, C. Fabre, and J. Laurat, “High-fidelity single-photon source based on a type II optical parametric oscillator,” *Opt. Lett.*, vol. 37, no. 17, p. 3738, 2012.

[5] L. D. Akulenko, S. V. Nesterov, and A. M. Shmatkov, “Generalized parametric oscillations of mechanical systems,” *J. Appl. Math. Mech.*, vol. 63, no. 5, pp. 705–713, Jan. 1999.

[6] R. Baskaran and K. Turner, “Mechanical domain non-degenerate parametric resonance in torsional mode micro electro mechanical oscillator,” in *Proc. 12th Int. Conf. Solid-State Sens., Actuators Microsyst. (TRANSDUCERS)*, 2003, pp. 863–866.

[7] R. C. Eckardt, C. D. Nabors, W. J. Kozlovsky, and R. L. Byer, “Optical parametric oscillator frequency tuning and control,” *J. Opt. Soc. Amer. B, Opt. Phys.*, vol. 8, no. 3, p. 646, Mar. 1991.

[8] L.-A. Wu, M. Xiao, and H. J. Kimble, “Squeezed states of light from an optical parametric oscillator,” *J. Opt. Soc. Amer. B, Opt. Phys.*, vol. 4, no. 10, p. 1465, Oct. 1987.

[9] T. J. Kippenberg, S. M. Spillane, and K. J. Vahala, “Kerr-nonlinearity optical parametric oscillation in an ultrahigh-QToroid microcavity,” *Phys. Rev. Lett.*, vol. 93, no. 8, pp. 18–21, Aug. 2004.

[10] I. S. Grudinin, A. B. Matsko, A. A. Savchenkov, D. Strekalov, V. S. Ilchenko, and L. Maleki, “Ultra high Q crystalline microcavities,” *Opt. Commun.*, vol. 265, no. 1, pp. 33–38, Sep. 2006.

[11] J. U. Fürst et al., “Low-threshold optical parametric oscillations in a whispering gallery mode resonator,” *Phys. Rev. Lett.*, vol. 105, no. 26, Dec. 2010, Art. no. 263904.

[12] X. Ji, “Ultra-low-loss on-chip resonators with sub-milliwatt parametric oscillation threshold,” *Optica*, vol. 4, no. 6, pp. 619–624, Jun. 2017.

[13] M. J. Seitner, M. Abdi, A. Ridolfo, M. J. Hartmann, and E. M. Weig, “Parametric oscillation, frequency mixing, and injection locking of strongly coupled nanomechanical resonator modes,” *Phys. Rev. Lett.*, vol. 118, no. 25, pp. 1–6, Jun. 2017.

[14] H. J. R. Westra, D. M. Karabacak, S. H. Brongersma, M. Crego-Calama, H. S. J. van der Zant, and W. J. Venstra, “Interactions between directly- and parametrically-driven vibration modes in a micromechanical resonator,” *Phys. Rev. B, Condens. Matter*, vol. 84, no. 13, pp. 1–4, Oct. 2011.

[15] C. Cassella and G. Piazza, “Low phase-noise autonomous parametric oscillator based on a 226.7 MHz AlN contour-mode resonator,” *IEEE Trans. Ultrason., Ferroelectr., Freq. Contr.*, vol. 62, no. 4, pp. 617–624, Apr. 2015.

[16] M. Park and A. Ansari, “Formation, evolution, and tuning of frequency combs in microelectromechanical resonators,” *J. Microelectromech. Syst.*, vol. 28, no. 3, pp. 429–431, Jun. 2019.

[17] M. Park and A. Ansari, “Phononic frequency combs in stand-alone piezoelectric resonators,” in *Proc. IEEE Int. Freq. Control Symp. (IFCS)*, May 2018, pp. 1–4.

[18] C. Li et al., “On enhancing the sensitivity of resonant thermometers based on parametric modulation,” *J. Microelectromech. Syst.*, vol. 30, no. 4, pp. 539–549, Aug. 2021.

[19] Y. Zhang, R. Kondo, B. Qiu, X. Liu, and K. Hirakawa, “Giant enhancement in the thermal responsivity of microelectromechanical resonators by internal mode coupling,” *Phys. Rev. Appl.*, vol. 14, no. 1, Jul. 2020, Art. no. 014019.

[20] N. C. Henry, D. Burghoff, and J. B. Khurgin, “Mitigating offset frequency drift in frequency combs using a customized power law dispersion,” *Opt. Lett.*, vol. 45, no. 13, p. 3525, 2020.

[21] S. Uetake, K. Matsubara, H. Ito, K. Hayasaka, and M. Hosokawa, “Frequency stability measurement of a transfer-cavity-stabilized diode laser by using an optical frequency comb,” *Appl. Phys. B, Lasers Opt.*, vol. 97, no. 2, pp. 413–419, Oct. 2009.

[22] J. Xi et al., “Multiple parameter decoupling for resonant MEMS sensors exploiting blue sideband excitation,” *J. Microelectromech. Syst.*, vol. 32, no. 5, pp. 426–436, Oct. 2023.

[23] J. Wang, M. Park, and A. Ansari, “Thermal characterization of ferroelectric aluminum scandium nitride acoustic resonators,” in *Proc. IEEE 34th Int. Conf. Micro Electro Mech. Syst. (MEMS)*, Jan. 2021, pp. 214–217.

[24] J. Wang, M. Park, S. Mertin, T. Pensala, F. Ayazi, and A. Ansari, “A high-k_t^2 switchable ferroelectric $Al_{0.7}Sc_{0.3}N$ film bulk acoustic resonator,” in *Proc. Joint Conf. IEEE Int. Freq. Control Symp. IEEE Int. Symp. Appl. Ferroelectr.*, Jul. 2020, pp. 1–3.

[25] J. Wang, M. Park, and A. Ansari, “High-temperature acoustic and electric characterization of ferroelectric $Al_{0.7}Sc_{0.3}N$ films,” *J. Microelectromech. Syst.*, vol. 31, no. 2, pp. 234–240, Apr. 2022.

[26] M. Park, Z. Hao, R. Dargis, A. Clark, and A. Ansari, “Epitaxial aluminum scandium nitride super high frequency acoustic resonators,” *J. Microelectromech. Syst.*, vol. 29, no. 4, pp. 490–498, Aug. 2020.

[27] Y. Zheng et al., “High-order Sezawa mode AlScN/GaN/sapphire surface acoustic wave resonators,” in *Proc. IEEE 35th Int. Conf. Micro Electro Mech. Syst. Conf. (MEMS)*, Jan. 2022, pp. 1046–1049.

[28] M. Moosavifar, A. Ansari, and M. Rais-Zadeh, “An AlN-on-Si resonant IR sensor array with a large temperature coefficient of frequency,” in *Proc. IEEE Sensors*, Nov. 2017, pp. 1–3.

[29] C. Tu, M.-H. Yang, Z.-Q. Zhang, X.-M. Lv, L. Li, and X.-S. Zhang, “Highly sensitive temperature sensor based on coupled-beam AlN-on-Si MEMS resonators operating in out-of-plane flexural vibration modes,” *Research*, vol. 2022, Jan. 2022, Art. no. 9865926.

[30] M.-H. Li, C.-Y. Chen, C.-S. Li, C.-H. Chin, and S.-S. Li, “Design and characterization of a dual-mode CMOS-MEMS resonator for TCF manipulation,” *J. Microelectromech. Syst.*, vol. 24, no. 2, pp. 446–457, Apr. 2015.

[31] C. M. Jha et al., “High resolution microresonator-based digital temperature sensor,” *Appl. Phys. Lett.*, vol. 91, no. 7, p. 74101, Aug. 2007.

Authorized licensed use limited to: Georgia Institute of Technology. Downloaded on April 29,2025 at 05:13:13 UTC from IEEE Xplore. Restrictions apply.

[32] J. L. Fu, R. Tabrizian, and F. Ayazi, "Dual-mode AlN-on-silicon micromechanical resonators for temperature sensing," *IEEE Trans. Electron Devices*, vol. 61, no. 2, pp. 591–597, Feb. 2014.

[33] X. C. Zhang, E. B. Myers, J. E. Sader, and M. L. Roukes, "Nanomechanical torsional resonators for frequency-shift infrared thermal sensing," *Nano Lett.*, vol. 13, no. 4, pp. 1528–1534, Apr. 2013.

[34] J. R. Vig, "Dual-mode oscillators for clocks and sensors," in *Proc. IEEE Ultrason. Symp. Int. Symp.*, vol. 2, Jun. 1999, pp. 859–868.

[35] J. A. Giordmaine and R. C. Miller, "Tunable coherent parametric oscillation in $LiNbO_3$ at optical frequencies," *Phys. Rev. Lett.*, vol. 14, no. 24, pp. 973–976, 1965.

[36] Keysight. *N9030B PXA X-Series Signal Analyzer, Multi-Touch | Keysight*. Accessed: Jun. 9, 2024. [Online]. Available: https://www.keysight.com/us/en/assets/7018-05093/data-sheets/5992-1317.pdf

[37] D. Wang et al., "Ferroelectric C-axis textured aluminum scandium nitride thin films of 100 nm thickness," in *Proc. Joint Conf. IEEE Int. Freq. Control Symp. Int. Symp. Appl. Ferroelectr. (IFCS-ISAF)*, Jul. 2020, pp. 1–4.

[38] S. Mishin and Y. Oshmyansky, "Stress control for highly doped aluminum scandium nitride films," in *Proc. IEEE Int. Ultrason. Symp. (IUS)*, Oct. 2018, pp. 1–9.

[39] G. Piazza, P. J. Stephanou, and A. P. Pisano, "Piezoelectric aluminum nitride vibrating contour-mode MEMS resonators," *J. Microelectromech. Syst.*, vol. 15, no. 6, pp. 1406–1418, Dec. 2006.

[40] X. Zhao, O. Kaya, M. Pirro, S. Kang, and C. Cassella, "Improving thermal linearity and quality factor of $Al_{72}Sc_{28}N$ contour mode resonators using acoustic metamaterials based lateral anchors," in *Proc. Joint Conf. Eur. Freq. Time Forum IEEE Int. Freq. Control Symp. (EFTF/IFCS)*, Apr. 2022, pp. 1–3.

[41] Y. Zheng, M. Park, A. Ansari, C. Yuan, and S. Graham, "Self-heating and quality factor: Thermal challenges in aluminum scandium nitride bulk acoustic wave resonators," in *Proc. 21st Int. Conf. Solid-State Sens., Actuators Microsyst. (Transducers)*, Jun. 2021, pp. 321–324.

[42] O. Wunnicke, P. J. van der Wel, R. C. Strijbos, and F. de Bruijn, "Thermal behavior of BAW filters at high RF power levels," *IEEE Trans. Ultrason., Ferroelectr., Freq. Control*, vol. 56, no. 12, pp. 2686–2692, Dec. 2009.

[43] A. Tazzoli, M. Rinaldi, and G. Piazza, "Experimental investigation of thermally induced nonlinearities in aluminum nitride contour-mode MEMS resonators," *IEEE Electron Device Lett.*, vol. 33, no. 5, pp. 724–726, May 2012.

[44] A. Lozzi, E. Ting-Ta Yen, P. Muralt, and L. G. Villanueva, "$Al_{0.83}Sc_{0.17}N$ contour-mode resonators with electromechanical coupling in excess of 4.5%," *IEEE Trans. Ultrason., Ferroelectr., Freq. Control*, vol. 66, no. 1, pp. 146–153, Jan. 2019.

[45] M. Reusch, K. Holc, V. Lebedev, N. Kurz, A. Žukauskaitė, and O. Ambacher, "Temperature cross-sensitivity of AlN-based flexural plate wave sensors," *IEEE Sensors J.*, vol. 18, no. 19, pp. 7810–7818, Oct. 2018.

[46] W. Sui, X.-Q. Zheng, J.-T. Lin, B. W. Alphenaar, and P. X.-L. Feng, "Thermal response and TC f of GaN/AlN heterostructure multimode micro string resonators from -10 °C up to 325 °C," *J. Microelectromech. Syst.*, vol. 30, no. 4, pp. 521–529, Aug. 2021.

[47] M. Ghatge and R. Tabrizian, "Bilayer nano-waveguide resonators for sensing applications," in *Proc. IEEE SENSORS*, Jan. 2016, pp. 1–3.

[48] W.-T. Hsu, J. R. Clark, and C. T.-C. Nguyen, "Mechanically temperature-compensated flexural-mode micromechanical resonators," in *IEDM Tech. Dig.*, Dec. 1999, pp. 399–402.

[49] R. Melamud et al., "Effects of stress on the temperature coefficient of frequency in double clamped resonators," in *Proc. 13th Int. Conf. Solid-State Sens., Actuators Microsyst. (TRANSDUCERS)*, Seoul, South Korea, pp. 392–395.

[50] COMSOL. *Residual Stress in a Thin-Film Resonator—3D*. Accessed: Feb. 12, 2024. [Online]. Available: https://www.comsol.com/model/residual-stress-in-a-thin-film-resonator-8212-3d-477

[51] Y. Lu et al., "Elastic modulus and coefficient of thermal expansion of piezoelectric $Al_{1-x}Sc_xN$ (up to x = 0.41) thin films," *APL Mater.*, vol. 6, no. 7, 2018, Art. no. 076105.

[52] R. B. Karabalin, R. Lifshitz, M. C. Cross, M. H. Matheny, S. C. Masmanidis, and M. L. Roukes, "Signal amplification by sensitive control of bifurcation topology," *Phys. Rev. Lett.*, vol. 106, no. 9, Feb. 2011, Art. no. 094102.

[53] M. Vainio and L. Halonen, "Mid-infrared optical parametric oscillators and frequency combs for molecular spectroscopy," *Phys. Chem. Chem. Phys.*, vol. 18, no. 6, pp. 4266–4294, 2016.

[54] Z. Liu et al., "Amplitude deflection in a nonlinear MEMS resonator under parametric excitation," *Int. J. Non-Linear Mech.*, vol. 163, Jul. 2024, Art. no. 104754.

[55] W.-M. Zhang and G. Meng, "Nonlinear dynamic analysis of electrostatically actuated resonant MEMS sensors under parametric excitation," *IEEE Sensors J.*, vol. 7, no. 3, pp. 370–380, Mar. 2007.

[56] K. Khirallah, "Parametric excitation, amplification, and tuning of MEMS folded-beam comb drive oscillator," *J. Microelectromech. Syst.*, vol. 22, no. 2, pp. 318–330, Apr. 2013.

[57] L. S. Cao, D. X. Qi, R. W. Peng, M. Wang, and P. Schmelcher, "Phononic frequency combs through nonlinear resonances," *Phys. Rev. Lett.*, vol. 112, no. 7, Feb. 2014, Art. no. 075505.

[58] A. Ganesan and A. Seshia, "Resonance tracking in a micromechanical device using phononic frequency combs," *Sci. Rep.*, vol. 9, no. 1, pp. 1–7, Jul. 2019, doi: 10.1038/s41598-019-46003-3.

[59] P. Thiruvenkatanathan, J. Woodhouse, J. Yan, and A. A. Seshia, "Manipulating vibration energy confinement in electrically coupled microelectromechanical resonator arrays," *J. Microelectromech. Syst.*, vol. 20, no. 1, pp. 157–164, Feb. 2011.

[60] H. Zhang et al., "A mode-localized MEMS accelerometer in the modal overlap regime employing parametric pump," in *Proc. 21st Int. Conf. Solid-State Sens., Actuators Microsyst. (TRANSDUCERS)*, Jun. 2021, pp. 108–111.

[61] C. Zhao et al., "Toward high-resolution inertial sensors employing parametric modulation in coupled micromechanical resonators," *Phys. Rev. Appl.*, vol. 12, no. 4, p. 1, Oct. 2019.

[62] P. Rafiee, G. Khatibi, and M. Zehetbauer, "A review of the most important failure, reliability and nonlinearity aspects in the development of microelectromechanical systems (MEMS)," *Microelectron. Int.*, vol. 34, no. 1, pp. 9–21, Jan. 2017.

[63] V. Kaajakari, T. Mattila, A. Lipsanen, and A. Oja, "Nonlinear mechanical effects in silicon longitudinal mode beam resonators," *Sens. Actuators A, Phys.*, vol. 120, no. 1, pp. 64–70, Apr. 2005, doi: 10.1016/j.sna.2004.11.010.

[64] M. I. Dykman, G. Rastelli, M. L. Roukes, and E. M. Weig, "Resonantly induced friction and frequency combs in driven nanomechanical systems," *Phys. Rev. Lett.*, vol. 122, no. 25, Jun. 2019, Art. no. 254301.

[65] C. Chen, D. H. Zanette, D. A. Czaplewski, S. Shaw, and D. López, "Direct observation of coherent energy transfer in nonlinear micromechanical oscillators," *Nature Commun.*, vol. 8, no. 1, pp. 1–7, May 2017.

Yue Zheng (Graduate Student Member, IEEE) received the B.S. and M.S. degrees from Georgia Institute of Technology, Atlanta, GA, USA, in 2019 and 2022, respectively, where she is currently pursuing the Ph.D. degree with the School of Electrical and Computer Engineering. Her current research interests include thermal sensing techniques, thermal modeling, and power handling of III–V compound semiconductor MEMS-based acoustic resonators.

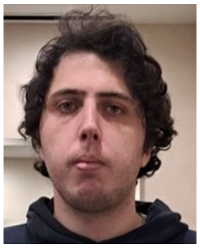

Seyyed Mojtaba Hassani Gangaraj (Graduate Student Member, IEEE) received the bachelor's degree in mechanical engineering from the K. N. Toosi University of Technology, Iran, in 2018, and the master's degree in mechanical engineering from the Sharif University of Technology, Iran, in 2021. He is currently pursuing the Ph.D. degree in electrical engineering with Georgia Institute of Technology, Atlanta, GA, USA. His research interests include MEMS resonators and mechanical frequency combs.

Authorized licensed use limited to: Georgia Institute of Technology. Downloaded on April 29,2025 at 05:13:13 UTC from IEEE Xplore. Restrictions apply.

Jialin Wang (Graduate Student Member, IEEE) received the B.S. and M.S. degrees from Georgia Institute of Technology, Atlanta, GA, USA, in 2017 and 2019, respectively, where he is currently pursuing the Ph.D. degree with the School of Electrical and Computer Engineering. His current research interests include the design and fabrication of III–V compound semiconductor MEMS resonators and filters.

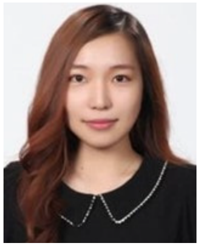

Mingyo Park (Member, IEEE) received the B.S. and M.S. degrees in electrical and electronic engineering from Yonsei University, Seoul, South Korea, in 2014 and 2016, respectively, and the Ph.D. degree in electrical and computer engineering from Georgia Institute of Technology (GT) in 2022. She joined the Department of Electrical Engineering, Pennsylvania State University (PSU), as an Assistant Professor, in Fall 2024. Previously, she was a Post-Doctoral Fellow with GT. Her research interests include the development of novel nano/microelectromechanical system (N/MEMS) devices utilizing aluminum scandium nitride piezoelectric material for acoustic resonators, targeting 5G filtering applications, and advanced sensing technologies.

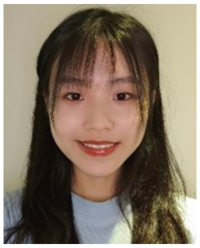

Yifan Fang (Graduate Student Member, IEEE) received the B.S. degree in electrical engineering from the University of Toronto, Canada, in 2020, and the master's degree from the School of Electrical and Computer Engineering, Georgia Institute of Technology, in 2023. Her master's thesis topic was phononic frequency combs.

Azadeh Ansari (Member, IEEE) received the B.S. degree in electrical engineering from the Sharif University of Technology, Tehran, Iran, in 2010, and the M.S. and Ph.D. degrees in electrical engineering from the University of Michigan, Ann Arbor, in 2013 and 2016, respectively, with a focus on III–V semiconductor and MEMS devices and microsystems for RF applications. She is currently an Associate Professor with the School of Electrical and Computer Engineering, Georgia Institute of Technology. Prior to joining the ECE Faculty, she was a Post-Doctoral Scholar with the Department of Physics, California Institute of Technology. Her research interests include nano/microelectromechanical systems (N/MEMS) and radio frequency (RF) integrated systems. She was a recipient of the 2023 Transducers Early Career Award, the 2022 Roger Webb Outstanding Junior Faculty Award, the 2019 NSF CAREER Award, and the 2017 ProQuest Distinguished Dissertation Award from the University of Michigan. She received the University of Michigan Richard and the Eleanor Towner Prize for Outstanding Ph.D. Research in 2016.

Authorized licensed use limited to: Georgia Institute of Technology. Downloaded on April 29,2025 at 05:13:13 UTC from IEEE Xplore. Restrictions apply.